Scientia Iranica B (2012) 19 (6), 1493–1501

Sharif University of Technology

Scientia Iranica

Transactions B: Mechanical Engineering

www.sciencedirect.com

Bifurcation analysis in hunting dynamical behavior in a railway bogie: Using novel exact equivalent functions for discontinuous nonlinearities

Hamid M. Sedighi *, **Kourosh H. Shirazi**

Department of Mechanical Engineering, Shahid Chamran University, Ahvaz, 61357-43337, Iran

Received 28 November 2011; revised 6 March 2012; accepted 16 September 2012

KEYWORDS

Hunting;
Rail wheelset;
Hopf bifurcation;
Discontinuous nonlinearity;
Routh–Hurwitz criterion;
Equivalent function;
Analytical approach.

Abstract This paper presents an investigation on bifurcation of railway bogie behavior in the presence of nonlinearities which are yaw damping forces in longitudinal suspension system and the friction creepage model of the wheel/rail contact including clearance. Through Routh–Hurwitz stability criterion and a more accurate model than Yang and Ahmadian, the analytical expression of critical speed is achieved as well as the limit cycle frequency. Then, by Averaging method and analytical critical speed, the amplitude of the limit cycle is determined while the wheel/rail clearance is taken into account. To solve the nonlinear equations analytically, both dead zone discontinuity and yaw dampers must be formulated properly. In this direction, a suitable and novel exact equivalent functions (EF) is introduced. Furthermore, 2D and 3D bifurcation diagrams are depicted to show the mechanism creation of Hopf bifurcation which is employed in the design of stable wheelset systems. Finally, the accuracy of one-axle model results for the prediction of critical speed is evaluated in contrast with two-axle bogie model.

1. Introduction

The dynamic response of High-speed railway vehicles under rail loads such as clearances between wheel/rail, the wheel flange contacting forces and dry friction in suspension components is one of the fundamental problems to be solved in railway vehicles design and maintenance. As the velocity of rail vehicle increases, the vehicle becomes less stable and ultimately exhibits rigorous oscillations. This is due to the velocity dependence of rail vehicle lateral and yaw stability, commonly known as "hunting". When flanging occurs, the motion is highly nonlinear due to the effects of wheel/rail contact forces as well as wheel clearance. Hence, the analysis of the influence of the rail vehicle parameters on the hunting motion is necessary to design safe vehicles.

Hunting is characterized by a limit cycle-type oscillation. It has been only in the last two decades that analyses have been made incorporating some of the more important nonlinearities that lead to the occurrence of the hunting, such as clearances between the components, the wheel flange contacting forces, dry friction in suspension components, etc..

Shabana et al. [1] investigated the effect of the approximations made in some of the creepage expressions and linearization of the kinematic equations in railroad vehicle system dynamics. The effect of wheel profiles on contact geometry in railroad turnout section was studied by Sugiyama et al. [2]. A dynamic characteristic of independently rotating-wheel systems in the analysis of multibody railroad vehicles was considered by Sugiyama et al. [3]. Abood and Khan [4] derived the mathematical model of a railway carriage moving on tangent tracks to study the influence of vertical secondary suspension stiffness on ride comfort of railway carbody. In order to describe the wheel and the rail contact patch area, they use linear Kalker's theory and non-linear Heuristic model. The dynamics of suspensions with friction that are widely used in three-piece bogie wagons was studied by Sun and Cole [5].

De-Pater [6] used Bogoliubov Averaging Method [7] to examine limit cycle behavior of a two-axle bogie with cylindrical wheels. Law and Brand [8] used the same method to analyze

* Corresponding author. Tel.: +98 6113330010x5665; fax: +98 6113336642.
E-mail addresses: hmsedighi@gmail.com, h-msedighi@phdstu.scu.ac.ir (H.M. Sedighi), k.shirazi@scu.ac.ir (K.H. Shirazi).

Peer review under responsibility of Sharif University of Technology.

Production and hosting by Elsevier

1026-3098 © 2012 Sharif University of Technology. Production and hosting by Elsevier B.V. Open access under CC BY-NC-ND license.
doi:10.1016/j.scient.2012.10.028

the dynamics of a single wheelset having curved wheel profiles and flange contact, where they modeled the effects of this flange force by a linear rail spring with a dead band equal to the flange clearance. Optimizing air suspension system of a complete four-axle rail vehicle model with 70 degrees of freedom using GA has been investigated by Sayyaadi and Shokouhi [9] to minimize the Sperling ride comfort index. Zou et al. [10] studied a dynamic computational model for the embedded railway track subjected to a moving load. Their model consists of two-layer Euler–Bernoulli beams and continuous viscoelastic elements. The resonance characteristics of a two-span continuous beam traversed by moving high-speed trains at a constant velocity have been developed by Wang et al. [11]. A dynamic model for analyzing the vibration of a train-track system investigated by Shi and Wang [12] and Zakeri et al. [13]. The Hopf bifurcation analysis in a rail bogie has been investigated by several researchers [14–18]. Pombo and Ambrósio [19] studied the implementation of a multi-joint wheel-rail contact model to railway dynamics in small radius curved tracks. The stress distribution in the rail, wheelset and subgrade has been studied by Sadeghi [20]. Sayyaadi and Shokouhi [21] introduced a complete nonlinear thermo-dynamical air spring model to optimize the ride comfort of passenger's index using a combination of two different models. Asadi Lari and Rezvani [22] focused on the development of a harmonic (lateral) wear pattern within the circumference of the wheel flanges. The effect of fluid damping in semi-active hydraulic dampers of railway bogie was studied by Wang and Xu [23].

Sedighi et al. [24–28] and Sedighi and Shirazi [29] modeled the dead zone nonlinearity and other discontinuities using continuity-based function to facilitate the severe computational issues that are encountered in the analytical investigations of nonlinear problems. Yang and Ahmadian [30] analyzed Hopf bifurcation in a wheelset in the presence of nonlinear yaw damper in primary suspension system. It was noted that the amplitude of the hunting limit cycle is large enough that the lateral wheel/rail flange force is created. Hence, it is necessary to include the flange contact forces in the model.

The flange force is modeled as a linear spring besides a nonlinear fourth order damping including a dead zone due to the wheel/rail clearance. This investigation emphasizes the influences of the system suspension nonlinearities and the wheel/rail interface nonlinearities on Hopf bifurcation. Frequency of the limit cycle and critical velocity are found analytically. Also using the Averaging method, a relation between the limit cycle amplitude and parameters of the system is introduced. These relations lead to several analytical criteria for prediction of possibility of hunting behavior. Two and three dimensional bifurcation diagrams to study the Hopf bifurcation in the system are demonstrated.

2. Governing equations of motion of single-axle wheelset

The wheelset is considered to be four degrees of freedom system and illustrates in Figure 1. The equations of motion are organized using Newton's second law of motion for y, ψ, z and φ as follows:

$$\begin{aligned} m_w\ddot{y} &= F_{ly} + F_{ry} - N_r \sin(\beta_r - \varphi) \\ &\quad + N_l \sin(\beta_l + \varphi) + F_{s,y} - F_T, \end{aligned} \tag{1}$$

$$\begin{aligned} &I_{wz}\ddot{\psi} - \left(I_{wx} - I_{wy}\right)\dot{\varphi}\dot{\theta} = a\left(F_{rx} - F_{lx}\right) \\ &\quad - a\psi\left[N_r \sin(\beta_r - \varphi) + N_l \sin(\beta_l + \varphi)\right] + M_{zr} \\ &\quad + M_{zl} + a\psi\left(F_{ry} - F_{ly}\right) + M_{s,z} - 2bF_d \end{aligned} \tag{2}$$

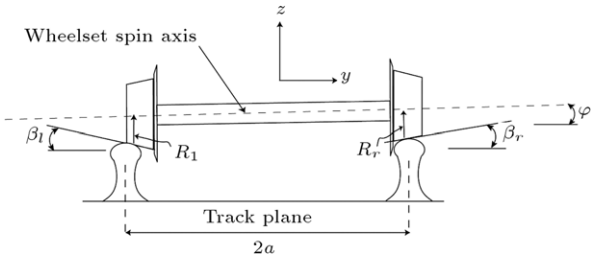

Figure 1: Free-body diagram for wheelset.

$$\begin{aligned} &I_{wx}\ddot{\varphi} - \left(I_{wy} - I_{wz}\right)\dot{\theta}\dot{\psi} = [N_r \sin(\beta_r - \varphi)\ R_r \\ &\quad - N_l \sin(\beta_l + \varphi)\ R_l] + \left(M_{yr} + M_{yl}\right)\psi \\ &\quad + a\left[-N_r \cos(\beta_r - \varphi) + N_l \cos(\beta_l + \varphi)\right] \\ &\quad + R_l\left[F_{lx}\psi - F_{ly}\right] + R_r\left[F_{rx}\psi - F_{ry}\right] + a\left[-F_{ry} + F_{lz}\right] \end{aligned} \tag{3}$$

$$\begin{aligned} m_w\ddot{z} &= F_{rz} + F_{lz} + N_r \cos(\beta_r - \varphi) \\ &\quad + N_l \cos(\beta_l + \varphi) - m_w g. \end{aligned} \tag{4}$$

The various creep forces and moments with respect to the left and right wheels were introduced by Sedighi and Shirazi [31], which F_{xp}, F_{yp}, M_{zp} are creep forces and moment of the wheelset, respectively and calculated as follows:

$$F_{xp} = -f_{33}\xi_x, \tag{5}$$

$$F_{yp} = -f_{11}\xi_y - f_{12}\xi_{sp}, \tag{6}$$

$$M_{zp} = f_{12}\xi_y - f_{22}\xi_{sp}. \tag{7}$$

For the constant forward velocity and straight rail the associated Kalker's creepages, for roll, pitch and yaw rates of the left and right contact planes are mentioned in Appendix C.

Figure 2 shows the suspension forces in the lateral direction, $F_{s,y}$, and the suspension moments in the vertical direction, $M_{s,z}$, acting on the wheelset which are induced from the lateral stiffness and the yaw damping of the primary suspension and can be expressed as follows:

$$F_{s,y} = -2K_y y - 2C_y\dot{y}, \tag{8}$$

$$M_{s,z} = -2K_x b^2\psi. \tag{9}$$

The nonlinear longitudinal yaw damping force F_d is considered according to the Yang and Ahmadian [30] assumptions as follows:

$$F_d = \begin{cases} C_1V_\psi + C_2{V_\psi}^2 + C_3{V_\psi}^3 + C_4{V_\psi}^4 & V_\psi > 0 \\ C_1V_\psi - C_2{V_\psi}^2 + C_3{V_\psi}^3 - C_4{V_\psi}^4 & V_\psi < 0. \end{cases} \tag{10}$$

Flange contact force F_T is described by the following formula:

$$F_T = \begin{cases} K_r(y - \delta) & y > \delta \\ 0 & -\delta \le y \le \delta \\ K_r(y + \delta) & y < -\delta \end{cases} \tag{11}$$

where $V_\psi = b\dot{\psi}$ is the relative velocity of the longitudinal yaw damper. The coefficients C_1 to C_4 are obtained from the experimental tests on the actual dampers by Yang and Ahmadian. The constant K_r is the wheel/rail contact lateral stiffness, and δ is the flange clearance. The lateral clearance is modeled as shown in Figure 3.

Assuming $\varphi = \lambda y/a, \dot{R} = \lambda\dot{\varphi}, R_l = R_r = R_0$, the vertical wheelset displacement equation of motion can be also neglected.

Solving Eqs. (3) and (4) for N_r and N_l and replacing them into Eqs. (1) and (2), the number of equations is reduced. Also, to

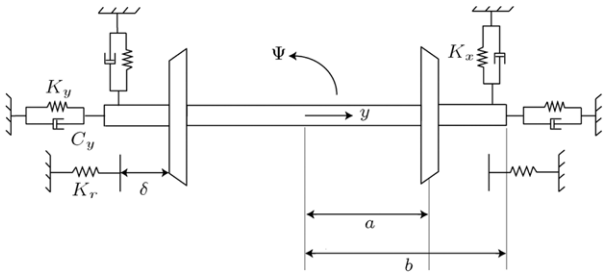

Figure 2: The wheelset model.

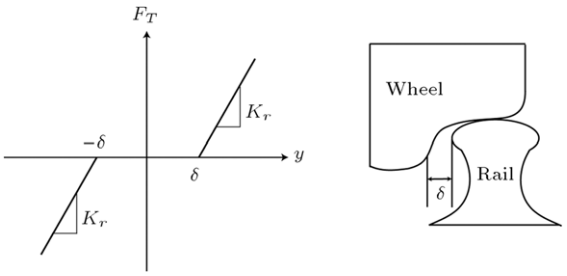

Figure 3: Flange force versus lateral displacement.

avoid emerging complicated terms, we can assume that angles are equal to their sines; thus, equations of motion reduced as follows:

$$m_w\ddot{y} + m_w g\lambda\frac{y}{a} + \frac{2f_{11}}{V}\left\{\left(1 + R_0\frac{\lambda}{a}\right)\dot{y} - V\psi\right\} + \frac{2f_{12}}{V}\left\{\dot{\psi} + \lambda\frac{y}{a}\frac{V}{R_0}\right\} = F_{s,y} - F_T, \tag{12}$$

$$I_{wz}\ddot{\psi} + \left(I_{wy} - I_{wx}\right)\frac{\lambda}{a}\frac{V}{R_0}\dot{y} + \frac{2af_{33}}{R_0}\lambda y - \frac{2f_{12}}{V}\left\{\left(1 + R_0\frac{\lambda}{a}\right)\dot{y} - V\psi\right\} + \frac{2a^2f_{33}}{V}\dot{\psi} - mg\lambda a\psi + \frac{2f_{22}}{V}\left\{\dot{\psi} + \dot{\theta}\,\lambda\frac{y}{a}\right\} = M_{s,z} - 2bF_d. \tag{13}$$

A comparison between Eq. (13) with Yang and Ahmadian's results indicated that the term $\left(I_{wy} - I_{wx}\right)\frac{\lambda}{a}\frac{V}{R_0}\dot{y}$ has been omitted and the Eulerian acceleration term has been deleted in their paper. As illustrated in the result section, this term change the critical speed of the system.

3. Critical speed of linear equation

To derive hunting velocity, the equations were changed to the state space form. Let us introduce state vector $X = \left\{y, \dot{y}, \psi, \dot{\psi}\right\}$ to represent the lateral and the yaw motion of the wheelset, so Eqs. (12) and (13) can be written in the general following form:

$$\dot{X} = A\left(V\right)X + F\left(X\right), \tag{14}$$

where $F\left(X\right)$ represents the nonlinear terms that should be modeled properly for analytical solution, and the elements of the matrix $A\left(V\right)$ are described in Appendix A.

To obtain critical speed V_c, Eq. (14) should be perturbed using ε which is a small perturbation coefficient as follows:

$$V = V_c + \varepsilon\mu$$
$$A\left(V\right) = A_0\left(V_c\right) + \varepsilon\mu A_1\left(V_c\right) + \left(\varepsilon\mu\right)^2 A_2\left(V_c\right) + \cdots \tag{15}$$

Table 1: Routh–Hurwitz criterion.

s^4	$a_4\left(V_c\right)$	$a_2\left(V_c\right)$	$a_0\left(V_c\right)$
s^3	$a_3\left(V_c\right)$	$a_1\left(V_c\right)$	
s^2	$b_1\left(V_c\right)$	$b_2\left(V_c\right)$	
s^1	$b_3\left(V_c\right)$		
s^0	$b_4\left(V_c\right)$		

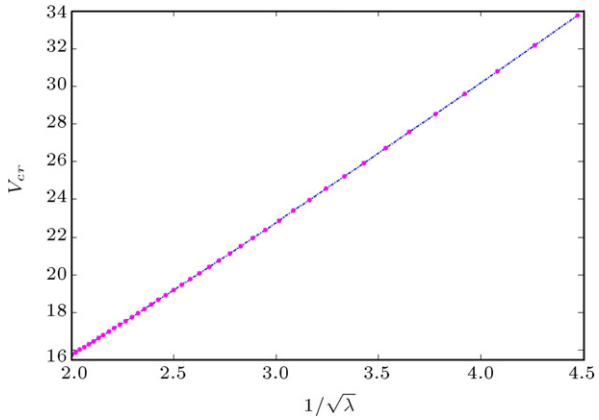

Figure 4: Theoretical critical speed versus $1/\sqrt{\lambda}$.

where μ indicates the perturbation of the forward speed V, $A_0\left(V_c\right)$ is matrix $A\left(V\right)$ in (23) when $V = V_c$. It is clear that in the presence of hunting behavior the matrix should possess at least a pair of purely imaginary eigenvalues denoted by $\pm i\omega$, and all other eigenvalues have negative real parts, where ω is the hunting frequency. Applying Routh–Hurwitz method for $|A_0 - sI|$, the following fourth order equation is obtained:

$$|A_0 - sI| = a_4\left(V_c\right)s^4 + a_3\left(V_c\right)s^3 + a_2\left(V_c\right)s^2 + a_1\left(V_c\right)s + a_0\left(V_c\right). \tag{16}$$

For marginally stability of the system, one zero element in the first column is required.

Setting the fourth equation in the first column of Table 1 equal to zero returns to a real valued solution for V_c. For parameters assumed in Appendix B, $V_{c,th}$ yields:

$$V_{c,th} = 40.1\ \text{m/s}. \tag{17}$$

Comparing between $V_{c,th}$ and that of obtained from simulation which is $V_c = 44.4$ m/s, indicated that the relative error is 9.7%. From Figure 4 it is seen that there is a linear relationship between the critical speed and $1/\sqrt{\lambda}$.

4. Asymptotic behavior of the nonlinear model

Based on the obtained results for V_c and ω, the nonlinear behavior of the system can be analyzed using the Bogoliubov Averaging method. Expanding $A\left(V\right)$ about V_c and combining Eqs. (12) and (13) give:

$$\dot{X} = A_0\left(V_c\right)X + \varepsilon F_1\left(X, \mu, \varepsilon\right), \tag{18}$$

where

$$F_1\left(X, \mu, \varepsilon\right) = BX + F\left(X\right) = \left\{0, f_2, 0, f_4\right\}^T, \tag{19}$$

in which the parameters f_2, f_4 are described in Appendix A. The eigenvectors of $A_0\left(V_c\right)$ and $A_0^T\left(V_c\right)$ corresponding to $\pm i\omega$ are $\xi_{12} = \alpha \pm i\beta$ and $\eta_{12} = p + iq$, respectively. Using the

Bogoliubov averaging method, we can obtain the approximate solution of Eq. (18) as follows:

$$X = 2a\left(\alpha\cos\varphi - \beta\sin\varphi\right) = 2a\sqrt{\alpha^2+\beta^2}\cos\left(\varphi+\gamma\right), \quad (20)$$

where $\gamma = tg^{-1}\left(\beta/\alpha\right)$ and the time dependent variables a and φ are defined as:

$$\frac{da}{at} = \varepsilon H_1\left(a\right), \quad (21a)$$

$$\frac{d\varphi}{dt} = \omega + \varepsilon G_1\left(a\right). \quad (21b)$$

Using symbolic calculations, the functions $H_1\left(a\right)$ and $G_1\left(a\right)$ can be expressed as:

$$H_1\left(a\right) = \frac{1}{2\pi}\int_{-\gamma}^{2\pi-\gamma}\sum_{i=1}^{2} f_{2\times i}\left(p_{2\times i}\cos\varphi + q_{2\times i}\sin\varphi\right)\,d\varphi, \quad (22a)$$

$$G_1\left(a\right) = \frac{1}{2\pi a}\int_{-\gamma}^{2\pi-\gamma}\sum_{i=1}^{2} f_{2\times i}\left(q_{2\times i}\cos\varphi - p_{2\times i}\sin\varphi\right)\,d\varphi. \quad (22b)$$

The steady state solution (limit cycle) occurred if $H_1\left(a\right) = 0$. Eq. (22) can be used to examine the amplitude and the phase of the limit cycle. To solve for the amplitude of the stationary limit cycle, we assume:

$$H_1\left(a\right) = \frac{1}{2\pi}\int_{-\gamma}^{2\pi-\gamma}\sum_{i=1}^{2} f_{2\times i}\left(p_{2\times i}\cos\varphi + q_{2\times i}\sin\varphi\right)\,d\varphi = 0, \quad (23)$$

which has the nontrivial solution a_1. To solve Eqs. (22) and (23) analytically as a function of a_1, two procedures are performed. In the first method, the equations are divided into three subdomain intervals shown as follows:

$$H_1\left(a\right) = \frac{1}{2\pi}\left(\int_{-\gamma}^{\cos^{-1}(S)-\gamma}\cdots d\varphi + \int_{\pi-\gamma-\cos^{-1}(S)}^{\pi-\gamma+\cos^{-1}(S)}\cdots d\varphi + \int_{2\pi-\cos^{-1}(S)}^{2\pi-\gamma}\cdots d\varphi\right) \quad (24)$$

where the term S in the integral domain is $\delta/2a\sqrt{\alpha^2+\beta^2}$. Functions f_2, f_4 are nonlinear functions in terms of dead zone and nonlinear yaw dampers. The second analytical method is based on the new formulation of dead zone and nonlinear yaw dampers. This approach enables us to overcome the inherent computational difficulty of this nonlinearity in the analytical investigations of nonlinear problems. We introduce suitable and novel exact equivalent function for these nonlinearities as:

$$F_d\left(V_\psi\right) = \left(\frac{1}{2}+\frac{1}{2}\frac{\left|V_\psi\right|}{V_\psi}\right)\times\left(C_1V_\psi + C_2{V_\psi}^2 + C_3{V_\psi}^3 + C_4{V_\psi}^4\right) + \left(\frac{1}{2}-\frac{1}{2}\frac{\left|V_\psi\right|}{V_\psi}\right)\times\left(C_1V_\psi - C_2{V_\psi}^2 + C_3{V_\psi}^3 - C_4{V_\psi}^4\right), \quad (25a)$$

$$F_T\left(y\right) = \frac{1}{2}K\left(2y + \left|y-\delta\right| - \left|y+\delta\right|\right). \quad (25b)$$

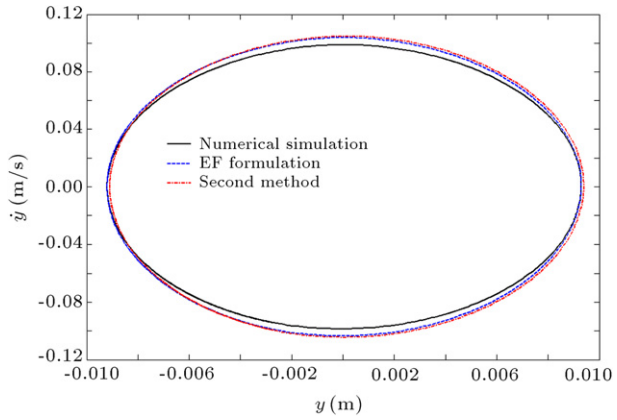

Figure 5a: A comparison of theoretical and numerical simulation for limit cycles of lateral displacement.

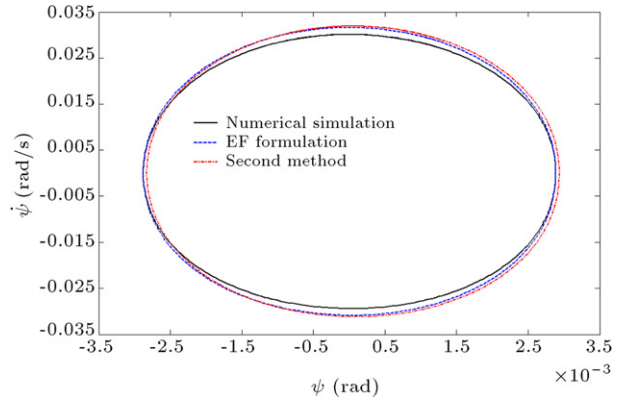

Figure 5b: A comparison of theoretical and numerical simulation for limit cycles of yaw rotation.

We obtained a_1 from Eq. (23) and substituted it in Eqs. (22) so we have:

$$\Omega = \omega + \frac{\varepsilon}{2\pi a}\times\int_{-\gamma}^{2\pi-\gamma}\sum_{i=1}^{2} f_{2\times i}\left(q_{2\times i}\cos\varphi - p_{2\times i}\sin\varphi\right)\,d\varphi. \quad (26)$$

Therefore, the long term behavior of the system can be obtained by substituting solution Eq. (23) for a into Eq. (20) that is given as follows:

$$X = 2a_1\sqrt{\alpha^2+\beta^2}\cos\left(\varphi+\gamma\right); \quad \varphi = \Omega t + \theta. \quad (27)$$

The variable θ is the phase shift determined by the initial conditions. It should be mentioned that in order to obtain Ω and X from Eq. (27) all the truncation terms are considered up to the second order ε in Eq. (15). A numerical example is illustrated in Figures 5a and 5b. Also, two theoretical as well as the numerical simulation limit cycle are indicated in Figures 5a and 5b. This figure demonstrates the accuracy of the asymptotic analytical procedures beside the soundness and effectiveness of the proposed EFs.

The limit cycle frequency obtained from numerical simulation is 10.578 rad/s and the theoretical one is 11.058 rad/s. A comparison between the frequencies shows that the theoretical analysis returns 4.5% error. The error has been calculated from the formulae $100\times\left|\omega_{th}-\omega_{si}\right|/\omega_{si}$ in which ω_{th} and ω_{si} are limit cycle frequencies obtained from the theoretical and numerical simulations, respectively.

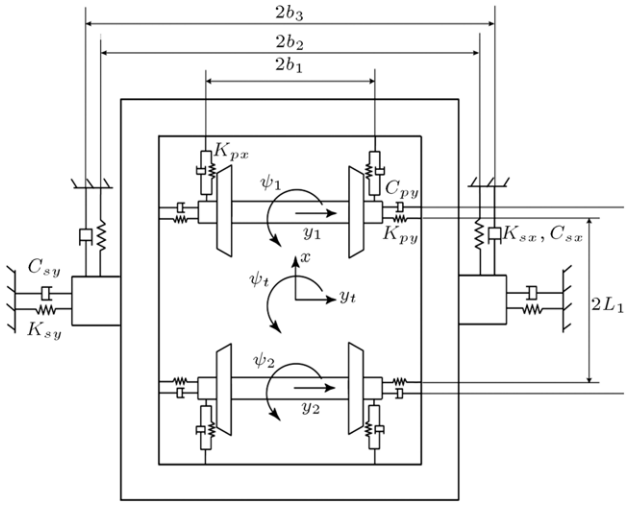

Figure 6: Two-axle model of bogie.

5. Governing equations of motion of two-axle wheelsets

Figure 6 illustrates the two-axle bogie model. The governing differential equations of four degrees of freedom obtained in the same method for single-axle model are given by:

Equation of motion for wheels in lateral direction:

$$m_w\ddot{y}_i + m_w g\lambda\frac{y_i}{a} + \frac{2f_{11}}{V}\left\{\left(1+R_0\frac{\lambda}{a}\right)\dot{y}_i - V\psi_i\right\} + \frac{2f_{12}}{V}\left\{\dot{\psi}_i + \lambda\frac{y_i}{a}\frac{V}{R_0}\right\} = F_{sus,yi} - F_{Ti}. \quad (28)$$

Equation of motion for wheels in yaw direction:

$$I_{wz}\ddot{\psi}_i + \left(I_y - I_x\right)\frac{\lambda}{a}\frac{V}{R_0}\dot{y}_i + \frac{2af_{33}}{R_0}\lambda y_i - \frac{2f_{12}}{V}\left\{\left(1+R_0\frac{\lambda}{a}\right)\dot{y}_i - V\psi_i\right\} + \frac{2a^2f_{33}}{V}\dot{\psi}_i - mg\lambda a\psi_i + \frac{2f_{22}}{V}\left\{\dot{\psi}_i + \dot{\theta}\lambda\frac{y_i}{a}\right\} = M_{sus,zi} - 2b_1F_{di} \quad (29)$$

where for rear axle $i = 1$ and for front axle $i = 2$. Parameters $F_{sus,yi}$ and $M_{sus,zi}$ are defined by:

$$F_{sus,yi} = -2K_y\left[y_i - y_t + (-1)^{i+1}l_1\psi_t\right] - 2C_y\left[\dot{y}_i - \dot{y}_t + (-1)^{i+1}l_1\dot{\psi}_t\right] \quad (30)$$

$$M_{sus,zi} = -2K_xb^2\left(\psi_i - \psi_t\right)$$

where y_t, ψ_t are lateral and yaw displacements of bogie and F_{Ti}, F_{di} are defined by:

$$F_{di} = \begin{cases} C_1V_{\psi_i} + C_2{V_{\psi_i}}^2 + C_3{V_{\psi_i}}^3 + C_4{V_{\psi_i}}^4 & V_{\psi_i} > 0 \\ C_1V_{\psi_i} - C_2{V_{\psi_i}}^2 + C_3{V_{\psi_i}}^3 - C_4{V_{\psi_i}}^4 & V_{\psi_i} < 0 \end{cases} \quad (31)$$

and:

$$F_{Ti} = \begin{cases} K_r\left(y_i - \delta\right) & y_i > \delta \\ 0 & -\delta \le y_i \le \delta \\ K_r\left(y_i + \delta\right) & y_i < -\delta. \end{cases} \quad (32)$$

And the governing equations of the motion of bogie are:

$$m_t\ddot{y}_t = -F_{sus,y1} - F_{sus,y2} - 2K_{ty}y_t - 2C_{ty}\dot{y}_t$$

$$I_{tz}\ddot{\psi}_t = -2K_y\left[y_1 - y_t + l_1\psi_t\right]l_1 + 2K_y\left[y_2 - y_t - l_1\psi_t\right]l_1 - 2C_y\left[\dot{y}_1 - \dot{y}_t + l_1\dot{\psi}_t\right]l_2 + 2C_y\left[\dot{y}_2 - \dot{y}_t - l_1\dot{\psi}_t\right]l_2 - 2K_{tx}b^2\psi_t - 2C_{tx}b_3^2\dot{\psi}_t + 2K_x\left(\psi_1 - \psi_2 - 2\psi_t\right) + 2b_1\left(F_{d1} + F_{d2}\right). \quad (33)$$

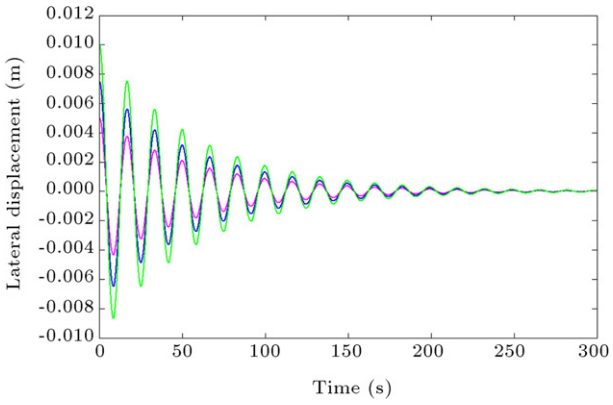

Figure 7a: Time response of lateral displacement at $V < V_c$.

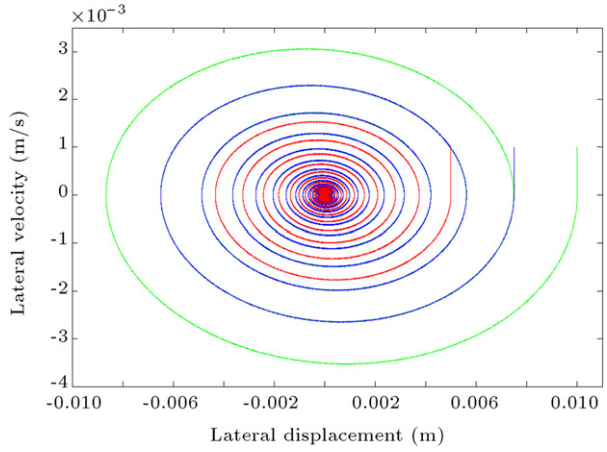

Figure 7b: Phase portrait of lateral displacement at $V < V_c$.

6. Results

As the velocity of rail vehicle increases, the vehicle becomes less stable and ultimately exhibits rigorous oscillations. In the viewpoint of bifurcation theory, hunting is a phenomenon called Hopf bifurcation of fixed point. The motion is stable below a certain "critical" forward velocity (or exhibits a stable fixed point in phase space). Above the critical speed, the hunting appears as an undamped vehicle motion constrained between the wheel flange and the rail (or the fixed point loses its stability and a limit cycle bifurcates from it). The decay rate of the phase portrait of wheelset depends on control parameter V. A supercritical Hopf bifurcation occurs when a stable spiral changes into an unstable spiral surrounded by a small limit cycle [32].

In Figures 7a–7d, the phase portrait and the time dependence of lateral displacement, for V above and below the critical bifurcation value V_c are illustrated. As can be seen, when $V < V_c$ the origin $y = 0$ is still a stable fixed point. For $V > V_c$, there is an unstable spiral at the origin and a stable circular limit cycle.

In order to analyze the influence of the system parameters on the hunting behavior, we solve Eqs. (12) and (13) numerically. By varying forward speed V and plot stable response of

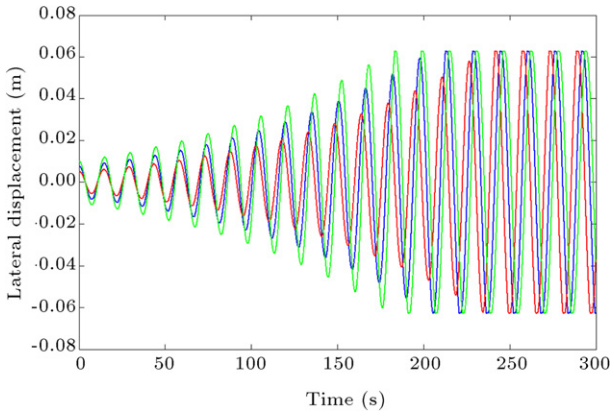

Figure 7c: Time response of yaw rotation at $V > V_c$.

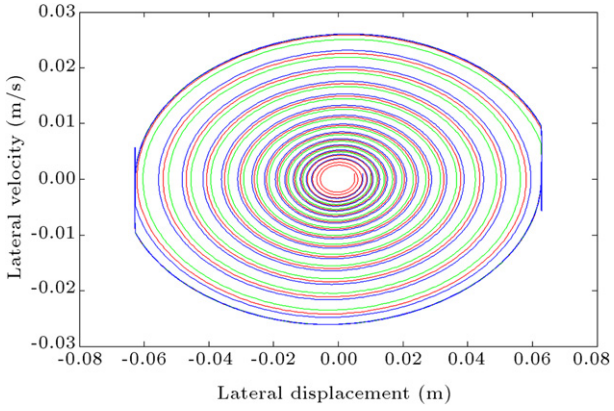

Figure 7d: Phase portrait of yaw rotation at $V > V_c$.

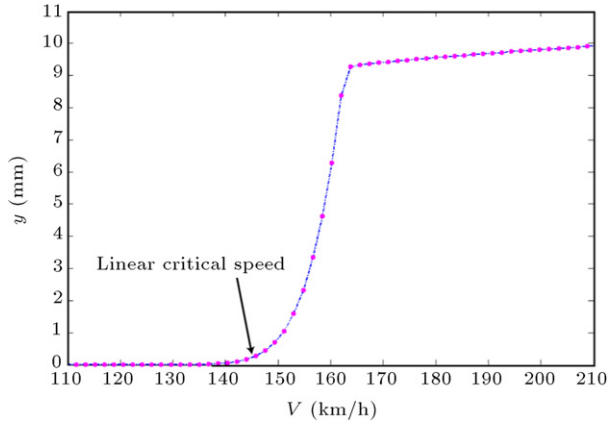

Figure 8: Bifurcation diagram for set of parameters value in Appendix B.

lateral displacement vs. speed, bifurcation diagrams are generated as shown in Figures 8–15. In Figure 8, the V_c obtained from Routh–Hurwitz criterion is depicted beside the direct numerical solution of the equation of motion. As this figure indicates, the V_c from numerical solution is 160 km/h while what is obtained from Routh–Hurwitz analysis is 145 km/h.

The effect of the rail stiffness (K_r) on the critical speed is considered. Figure 9 shows that the rail stiffness has no remarkable effect on hunting speed; however, it reduces hunting amplitude. Also, Figure 10 indicates that smaller flange clearance reduces the amplitude of limit cycle with no significant effects on critical speed.

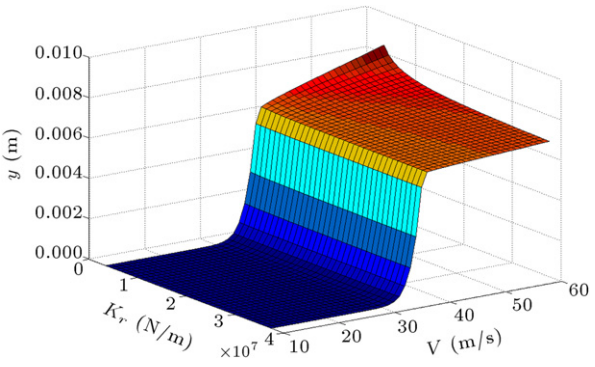

Figure 9: The effect of rail lateral stiffness on critical speed.

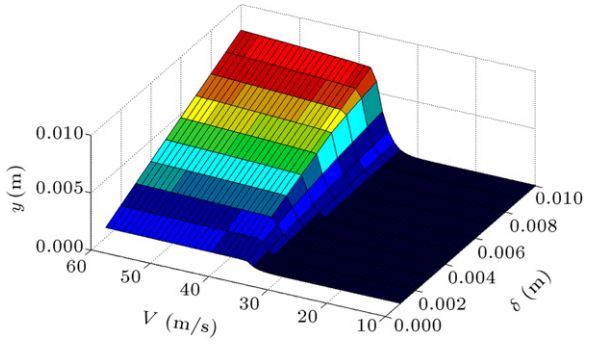

Figure 10: The effect of flange clearance on critical speed.

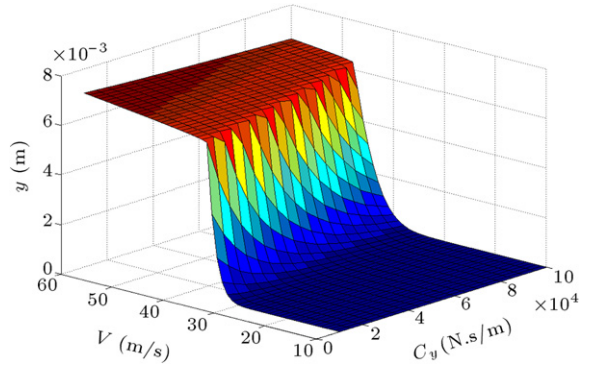

Figure 11: The effect of lateral damping on critical speed.

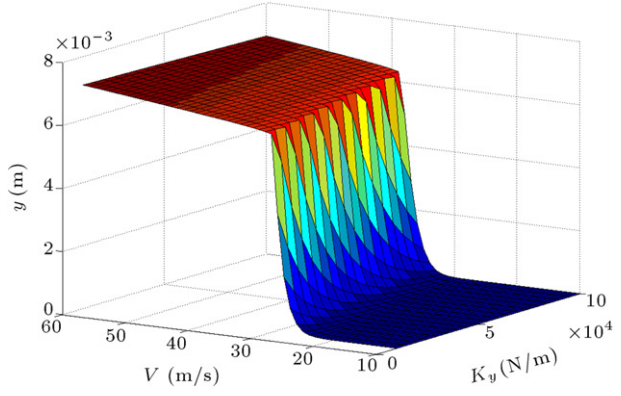

Figure 12: The effect of lateral spring stiffness on critical speed.

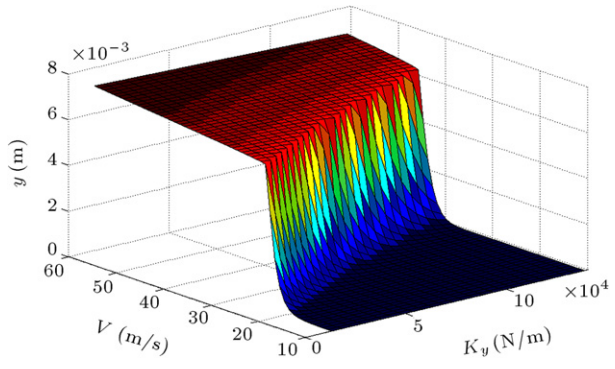

Figure 13: The effect of yaw spring stiffness on critical speed.

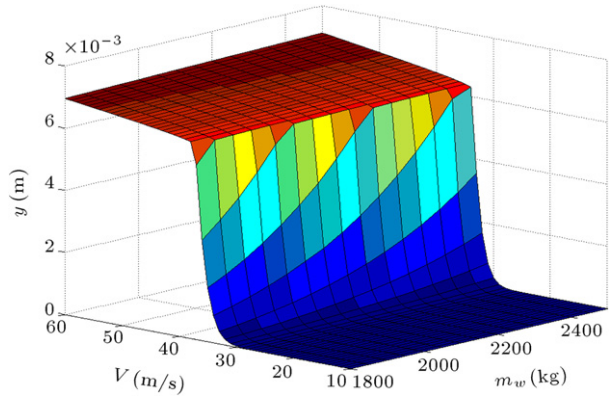

Figure 14: The effect of wheel-set mass on critical speed.

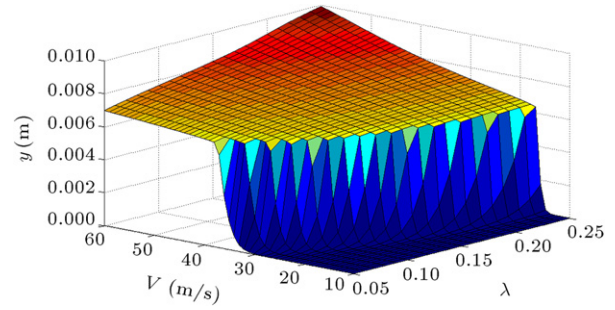

Figure 15: The effect of wheel-set conisity on critical speed.

Through Figures 11–15, the effect of variation of the parameters C_y, K_y, K_x, m_w and λ on critical speed is indicated.

Increasing lateral stiffness, as well as lateral damping and yaw stiffness, increases the critical speed V_c and decreases the hunting amplitude. Comparing Figures 11–13, it is seen that the hunting speed shows more sensitivity to change of the yaw stiffness relative to the other parameters such as the lateral damping.

As Figures 14 and 15 indicate, increasing wheelset mass as well as wheelset conicity decreases the critical speed V_c and increases the hunting amplitude while the hunting speed and hunting amplitude shows more sensitivity to change of the wheelset conicity relative to the wheelset mass.

7. Accuracy of one-axle model

To investigate the accuracy of one-axle wheelset model, the results of one and two-axles model for the same conditions,

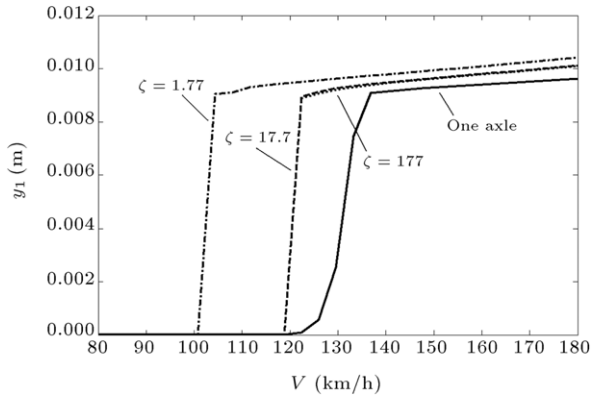

Figure 16: Effect of lateral dimensionless stiffness on accuracy of one-axle model.

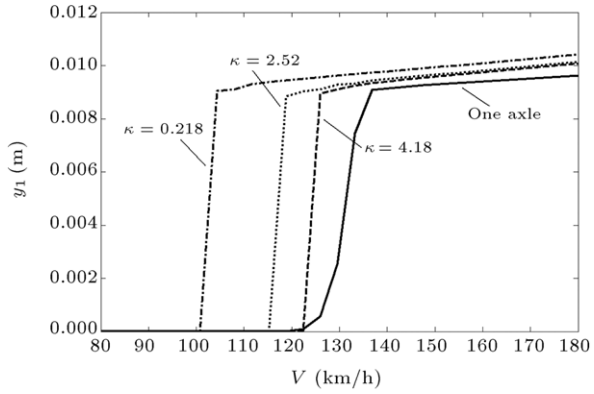

Figure 17: Effect of longitudinal dimensionless stiffness on accuracy of one-axle model.

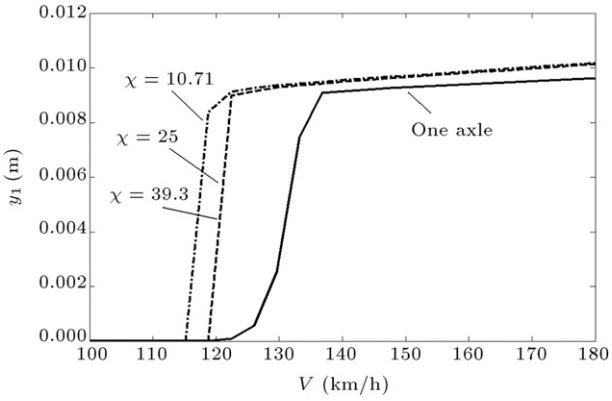

Figure 18: Effect of longitudinal dimensionless damping coefficient on accuracy of one-axle model.

have been compared. For this purpose, the dimensionless parameters are introduced as follows:

$\zeta = K_{ty}/K_y$ lateral dimensionless stiffness;
$\kappa = K_{tx}/K_x$ longitudinal dimensionless stiffness;
$\chi = C_{ty}/C_y$ longitudinal dimensionless damping coefficient.

Bifurcation diagrams for these parameters, as plotted in Figures 16–18, indicates that increasing these parameters makes one-axle model results in being more precise.

As shown in Figure 16, increasing lateral dimensionless stiffness from 1.77 to 17.7, has considerable effect on the

accuracy of one-axle model; however, it is not sensitive to more changes of lateral dimensionless stiffness (ζ). Changing the other dimensionless parameters κ and χ has the same impact on the accuracy of the first model, as indicated in Figures 17 and 18.

8. Conclusions

Hopf bifurcation in a railway wheelset was studied through a nonlinear model in this paper. The research assumed nonlinear lateral wheel/rail contact and also nonlinear yaw damper suspension elements. Novel EFs for these discontinuous nonlinearities have been employed to predict analytical response of nonlinear vibration in the time domain. It appears from the present work that the introduced EFs can significantly make the analytical investigation of the nonlinear problems to be estimated quite easily. The authors believe that the introduced procedure has special potential to be applied on other strong nonlinearities such as preload, dead zone and saturation discontinuous. Furthermore, the effect of primary suspension parameters such as lateral damping and stiffness, yaw stiffness, wheelset mass and wheelset conicity on critical speed were also investigated as summarized below:

1. The more gauge clearance, the less amplitude of hunting. However, gauge clearance does not have a significant effect on the critical speed.
2. Contrary to lateral damping which has little effect on the critical speed, yaw stiffness has a major effect on hunting velocity and can be an important design parameter.
3. Increasing the rail lateral stiffness does not significantly affect the critical speed, but reduces hunting amplitude.
4. As the wheel conicity increases, the critical speed reduces. As shown in Figure 4, linear critical speed obtained from Routh–Hurwitz criterion is proportional to $1/\sqrt{\lambda}$.
5. The results indicate that when the value of dimensionless parameters increases, the critical speed obtained from one-axle wheelset become more accurate.

Appendix A

The elements of matrix $A\,(V)$ are:

$$a_{21} = -\frac{1}{m_w}\left(2K_y + m_w g\frac{\lambda}{a}\right) \tag{A.1}$$

$$a_{22} = -\frac{2}{m_w}\left[C_y + \frac{f_{11}}{V}\left(1+\frac{R_0}{a}\right)\right] \tag{A.2}$$

$$a_{23} = -\frac{2f_{11}}{m_w} \tag{A.3}$$

$$a_{24} = -\frac{2f_{12}}{m_w} \tag{A.4}$$

$$a_{41} = -\frac{2af_{33}\lambda}{R_0 I_{wx}} \tag{A.5}$$

$$a_{42} = \frac{1}{I_{wx}}\left[-\frac{\lambda V}{R_0 a}\left(I_{wy}-I_{wx}\right) + \frac{2f_{12}}{V}\left(1+\frac{R_0\lambda}{a}\right)\right] \tag{A.6}$$

$$a_{43} = \frac{1}{I_{wx}}\left[am_w g\lambda - 2f_{12} - 2b^2K_x\right] \tag{A.7}$$

$$a_{44} = -\frac{1}{I_{wx}}\left[2bC_1 + \frac{2}{V}\left(a^2f_{33}+f_{22}\right)\right] \tag{A.8}$$

$$a_{12} = 1, \qquad a_{34} = 1. \tag{A.9}$$

Other elements of matrix A are zero.

$$f_2 = b_{22}x_2 + b_{24}x_4 - \frac{1}{m_w}F_T \tag{A.10}$$

$$f_4 = b_{42}x_2 + b_{44}x_4 - \frac{2b}{I_{wx}}F_d \tag{A.11}$$

$$b_{22} = -\frac{2f_{11}}{m_w}\left(1+\frac{R_0\lambda}{a}\right)\left(-\frac{\mu}{V_c^2} + \frac{\varepsilon\mu^2}{V_c^3} + \cdots\right) \tag{A.12}$$

$$b_{24} = -\frac{2f_{12}}{m_w}\left(-\frac{\mu}{V_c^2} + \frac{\varepsilon\mu^2}{V_c^3} + \cdots\right) \tag{A.13}$$

$$b_{42} = -\frac{2f_{12}}{I_{wx}}\left(1+\frac{R_0\lambda}{a}\right)\left(-\frac{\mu}{V_c^2} + \frac{\varepsilon\mu^2}{V_c^3} + \cdots\right) \tag{A.14}$$

$$b_{42} = -\frac{2}{I_{wx}}\left(a^2f_{33}+f_{22}\right)\left(-\frac{\mu}{V_c^2} + \frac{\varepsilon\mu^2}{V_c^3} + \cdots\right). \tag{A.15}$$

Appendix B

System parameters of the analysis mode are:

Half of the track gauge	$a = 0.7176$ m
Half of yaw spring arm	$b = 1$ m
Lateral damping of suspension	$C_y = 2.1\ e4$ N s/m
Damping coefficients for yaw dampers	$C_1 = 1.923\ e4$ $C_2 = 5.14\ e5$ $C_3 = -3.1127\ e6$ $C_4 = 5.14\ e6$
Lateral creep force coefficient	$f_{11} = 6.728\ e6$ N
Spin creep force coefficient	$f_{22} = 1000$ N m^2
Lateral spin creep force coefficient	$f_{12} = 1.2\ e3$ N m
Longitudinal creep force coefficient	$f_{33} = 6.728\ e6$ N
Roll moment of inertia of wheelset	$I_{wx} = 625.7$ kg m^2
Spin moment of inertia of wheelset	$I_{wy} = 133.92$ kg m^2
Lateral rail stiffness	$K_r = 1.617\ e7$ N/m
Lateral stiffness of primary suspension	$K_y = 8.67\ e4$ N/m
Yaw spring stiffness of primary suspension	$K_x = 8.67\ e4$ N/m
Wheelset mass	$m_w = 1800$ kg
Wheel radius	$R_0 = 0.533$ m
Wheel conicity	$\lambda = 0.05$
Flange clearance	$\delta = 0.923$ cm

Appendix C

The Kalker's creepage formula is:

$$\xi_{xl} = \frac{1}{V}\left[V - R_l\dot{\theta} - a\dot{\psi}\right] \tag{C.1}$$

$$\xi_{yl} = \frac{1}{V\cos\left(\beta_l+\varphi\right)}\left[\dot{y} + R_l\left(\dot{\varphi} - \dot{\theta}\,\psi\right)\right] \tag{C.2}$$

$$\xi_{spl} = \frac{1}{V}\left[-\dot{\theta}\sin\left(\beta_l+\varphi\right) + \left(\dot{\psi}+\varphi\,\dot{\theta}\right)\cos\left(\beta_l+\varphi\right)\right] \tag{C.3}$$

$$\xi_{xr} = \frac{1}{V}\left[V - R_r\dot{\theta} + a\dot{\psi}\right] \tag{C.4}$$

$$\xi_{yr} = \frac{1}{V\cos\left(\beta_r-\varphi\right)}\left[\dot{y} + R_r\left(\dot{\varphi} - \dot{\theta}\,\psi\right)\right] \tag{C.5}$$

$$\xi_{spr} = \frac{1}{V}\left[\dot{\theta}\sin\left(\beta_r-\varphi\right) + \left(\dot{\psi}+\varphi\,\dot{\theta}\right)\cos\left(\beta_r-\varphi\right)\right]. \tag{C.6}$$

References

[1] Shabana, A.A., Tobaa, M., Marquis, B. and El-Sibaie, M. "Effect of the linearization of the kinematic equations in railroad vehicle system dynamics", *ASME Journal of Computational and Nonlinear Dynamics*, 1(1), p. 25 (2006), http://dx.doi.org/10.1115/1.1951783.

[2] Sugiyama, H., Tanii, Y. and Matsumura, R. "Analysis of wheel/rail contact geometry on railroad turnout using longitudinal interpolation of rail profiles", *ASME Journal of Computational and Nonlinear Dynamics*, 6(2), p. 024501 (2011), http://dx.doi.org/10.1115/1.400234.

[3] Sugiyama, H., Matsumura, R., Suda, Y. and Ezaki, H. "Dynamics of independently rotating wheel system in the analysis of multibody railroad vehicles", *ASME Journal of Computational and Nonlinear Dynamics*, 6(1), p. 011007 (2011), http://dx.doi.org/10.1115/1.4002089.

[4] Abood, K.H.A. and Khan, R.A. "Railway carriage simulation model to study the influence of vertical secondary suspension stiffness on ride comfort of railway carbody", *Proceedings of the Institution of Mechanical Engineers, Part C: Journal of Mechanical Engineering Science*, 225(6), pp. 1349–1359 (2011), http://dx.doi.org/10.1177/0954406211399809.

[5] Sun, Y.Q. and Cole, C. "Comprehensive wagon-track modelling for simulation of three-piece bogie suspension dynamics", *Proceedings of the Institution of Mechanical Engineers, Part C: Journal of Mechanical Engineering Science*, 221(8), pp. 905–917 (2007), http://dx.doi.org/10.1243/09544062JMES434.

[6] De-Pater, A.D. "The approximate determination of the hunting movement of a railway vehicle by aid of the method of Krylov and Bogoliubov", *Applied Scientific Research A*, 10(1), pp. 205–228 (1960), http://dx.doi.org/10.1007/BF00411914.

[7] Bogoliubov, N.N. and Mitropolsky, Y.A., *Asymptotic Method in the Theory of Nonlinear Oscillations*, Hindustan Publishing Corp., Delhi, India pp. 158–192 (1961).

[8] Law, E.H. and Brand, R.S. "Analysis of the nonlinear dynamics of a railway vehicle wheelset", *ASME Journal of Dynamic Systems, Measurement and Control*, 95, pp. 28–35 (1973), http://dx.doi.org/10.1115/1.3426645.

[9] Sayyaadi, H. and Shokouhi, N. "New dynamics model for rail vehicles and optimizing air suspension parameters using GA", *Scientia Iranica, Transactions B*, 16(6), pp. 496–512 (2009).

[10] Zou, J.H., Feng, W.X. and Jiang, H.B. "Dynamic response of an embedded railway track subjected to a moving load", *Journal of Vibroengineering*, (ISSN: 1392-8716) 13(3), pp. 544–551 (2011).

[11] Wang, Y., Wei, Q.C., Shi, J. and Long, X. "Resonance characteristics of two-span continuous beam under moving high speed trains", *Latin American Journal of Solids and Structures*, 7, pp. 185–199 (2010).

[12] Shi, J. and Wang, Y.J. "Dynamic response analysis of single-span guideway caused by high speed maglev train", *Latin American Journal of Solids and Structures*, 8, pp. 213–228 (2011).

[13] Zakeri, J.A., Xia, H. and Fan, J.J. "Dynamic responses of train-track system to single rail irregularity", *Latin American Journal of Solids and Structures*, 6, pp. 89–104 (2009).

[14] Huilgol, R.R. "Hopf–Friedrichs bifurcation and the hunting of a railway axle", *Quarterly PMM Journal of Applied Mathematics and Mechanics*, 12, pp. 85–94 (1978).

[15] True, H. and Kaas-Petersen, C. "A bifurcation analysis of nonlinear oscillations in railway vehicles", *The Dynamics of Vehicles on Road and on Tracks, 8th IAVSD Symp.*, pp. 438–444 (1984).

[16] Chung, W.J. and Shim, J.K. "Influence factors on critical speed hysteresis in railway vehicles", *JSME International Journal*, 46, pp. 278–288 (2003).

[17] Kim, P. and Seok, J. "Bifurcation analysis on the hunting behavior of a dual-bogie railway vehicle using the method of multiple scales", *Journal of Sound and Vibration*, 329, pp. 4017–4039 (2010), http://dx.doi.org/10.1016/j.jsv.2010.03.024.

[18] Schupp, G. "Bifurcation analysis of railway vehicles", *Multibody System Dynamics*, 5, pp. 25–50 (2006), http://dx.doi.org/10.1007/s11044-006-2360-6.

[19] Pombo, J.C. and Ambrósio, J.C. "Application of a wheel-rail contact model to railway dynamics in small radius curved tracks", *Multibody System Dynamics*, 19, pp. 91–114 (2008).

[20] Sadeghi, J. "Investigation on modeling of railway track system", *Scientia Iranica*, 8(1), pp. 76–79 (2001).

[21] Sayyaadi, H. and Shokouhi, N. "Effects of air reservoir volume and connecting pipes' length and diameter on the air spring behavior in rail-vehicles", *Iranian Journal of Science and Technology, Transaction B: Engineering*, 34(B5), pp. 499–508 (2010).

[22] Asadi Lari, A. and Rezvani, M.A. "Observation of sinusoidal motion creating harmonic wavy pattern in the rail vehicle wheel flanges", *Iranian Journal of Science and Technology, Transaction B: Engineering*, 32(B4), pp. 315–324 (2008).

[23] Wang, W.L. and Xu, G.X. "Fluid formulae for damping changeability conceptual design of railway semi-active hydraulic dampers", *International Journal of Non-Linear Mechanics*, 44(7), pp. 809–819 (2009).

[24] Sedighi, H.M., Shirazi, K.H. and Zare, J. "Novel equivalent function for deadzone nonlinearity: applied to analytical solution of beam vibration using He's parameter expanding method", *Latin American Journal of Solids and Structures*, 9, pp. 443–451 (2012).

[25] Sedighi, H.M., Shirazi, K.H., Reza, A. and Zare, J. "Accurate modeling of preload discontinuity in the analytical approach of the nonlinear free vibration of beams", *Proceedings of the Institution of Mechanical Engineers, Part C: Journal of Mechanical Engineering Science*, 226(10), pp. 2474–2484 (2012), http://dx.doi.org/10.1177/0954406211435196.

[26] Sedighi, H.M., Reza, A. and Zare, J. "Dynamic analysis of preload nonlinearity in nonlinear beam vibration", *Journal of Vibroengineering*, (ISSN: 1392-8716) 13(4), pp. 778–787 (2011).

[27] Sedighi, H.M., Reza, A. and Zare, J. "Study on the frequency-amplitude relation of beam vibration", *International Journal of the Physical Sciences*, 6(36), pp. 8051–8056 (2011), http://dx.doi.org/10.5897/IJPS11.1556.

[28] Sedighi, H.M., Shirazi, K.H., Noghrehabadi, A.R. and Yildirim, A. "Asymptotic investigation of buckled beam nonlinear vibration", *Iranian Journal of Science and Technology, Transactions of Mechanical Engineering*, 36(M2), pp. 107–116 (2012).

[29] Sedighi, H.M. and Shirazi, K.H. "A new approach to analytical solution of cantilever beam vibration with nonlinear boundary condition", *ASME Journal of Computational and Nonlinear Dynamics*, 7, p. 034502 (2012), http://dx.doi.org/10.1115/1.4005924.

[30] Yang, S. and Ahmadian, M. "The Hopf bifurcation in a rail wheelset with nonlinear damping", *Proc. of Transportation Division, International Mechanical Engineering Congress and Exposition*, Atlanta., pp. 112–135 (1996).

[31] Sedighi, H.M. and Shirazi, K.H. "A survey of Hopf bifurcation analysis in nonlinear railway wheelset dynamics", *Journal of Vibroengineering*, (ISSN: 1392-8716) 14(1), pp. 344–351 (2012).

[32] Strogatz, S.H., *Nonlinear Dynamics and Chaos, with Application to Physics, Biology, Chemistry and Engineering*, Perseus Books Publishing (1994).

Hamid Mohammad Sedighi was born in 1983 in Iran. He is currently a Ph.D. student working under the supervision of Dr. Kourosh H. Shirazi in mechanical engineering at Shahid Chamran University of Ahvaz in Iran. He obtained his M.S. degree (2007) from Shahid Chamran University of Ahvaz and his undergraduate B.S. degree (2005) from Shiraz University. His general academic areas of interest include Mathematics, Nonlinear Dynamical Systems, Elasticity and Machine Design. As a teacher and a teaching Assistant, he has held various positions at SCU and IAU Ahvaz. The topic of his Ph.D. research is "Analysis of nonlinear dynamical behavior of multilayer beams with interlayer slip".

Kourosh Heidari Shirazi was born in 1969 in Iran. After studying in University of Science and Technology, he received a B.S. degree in mechanical engineering—solid mechanics in 1992. He pursued his study in mechanical engineering in Amirkabir University (Tehran Polytechnic) and received an M.S. degree in 1993 and Ph.D. degree in 2002. He started his work as a full time Faculty Member in Shahid Chamran University since 2002 until present. During his work he offered 7 courses such as Linear Control Theory, Design of Chassis and Body of Vehicle and Mechanisms Design in undergraduate program and 6 courses such as Advanced Dynamics, Advanced Mathematics and Nonlinear Dynamics in graduate program. His research interest is Kinematic of Mechanisms, Vehicle Dynamics and Chaotic Dynamics. He is a member of ASME and SAE.